Structural design model for tunnels in soft soils
From construction stages to the long-term

Vu, Minh Ngan; Broere, Wout

DOI
10.1016/j.tust.2018.04.017

Publication date
2018

Document Version
Final published version

Published in
Tunnelling and Underground Space Technology

Tunnelling and Underground Space Technology 78 (2018) 16–26

Contents lists available at ScienceDirect

Tunnelling and Underground Space Technology

journal homepage: www.elsevier.com/locate/tust

Structural design model for tunnels in soft soils: From construction stages to the long-term

Minh Ngan Vu[a,b,*], Wout Broere[a]

[a] Delft University of Technology, Geo-Engineering Section, Stevinweg 1, 2628 CN Delft, The Netherlands
[b] Hanoi University of Mining and Geology, Faculty of Civil Engineering, Viet Nam

ARTICLE INFO

Keywords:
Structure
Tunnel
Soft soils

ABSTRACT

In bored tunnel design, most recent structural design models for tunnel linings concentrate on the behaviour of the tunnel lining in the long-term. The load on the tunnel lining in these models is derived from the original soil stresses, often simplified for a single homogeneous layer. Field observations show that higher loads may occur in the initial hours after the assembly, that might effect the tunnel lining and that soil layers with different stiffnesses may have a negative impact on the internal forces of the tunnel lining. This paper proposes a new model for these early construction stages and also includes a more accurate model which explicitly models the impact of multilayered soils. The change of internal forces in the tunnel lining from the initial construction time to the long-term is investigated with this model. Validations with field observations and other analysis results at time of construction and the long-term confirm that the new structural analysis models can accurately predict internal forces in the tunnel lining. The analysis results also show that internal forces in the tunnel lining have an increasing trend in time and become stable in the long-term and accord with field observations.

1. Introduction

The increased use of Tunnel Boring Machines (TBMs) in constructing (urban) underground space (Broere, 2016) combined with the fact that most of the world urban population resides in coastal and delta areas, with often soft soil conditions, means that increasingly tunnels are bored in soft layered soils and with decreasing cover. Besides assessment of face stability, surface settlement and resulting damage to buildings (Vu, 2016), structural analysis of the tunnel lining remains an important issue in tunnelling design. However, the common simplifications of homogeneous soil conditions and homogeneous stress conditions in most structural design methods are less applicable for tunnels with limited cover in soft soils. There is a number of structural design models for the tunnel lining commonly used encompassing both analytical models and numerical models. The first analysis method for an elastic continuum was proposed by Schmid (1926). Morgan (1961) introduced an analytical continuum model, which considers the elliptical deformation of the tunnel lining. Then, Schulze and Duddeck (1964) produced a bedded ring model for analysing the case of shallow tunnels. Windels (1966) further developed the model proposed by Schulze and Duddeck (1964) by taking into account the second order of the series expansion of the analytical solution and the deformation of the tunnel lining in the construction stage. A design model for a circular tunnel in an elastic continuum with geometrical nonlinearity was presented by Windels (1967). The model proposed by Morgan (1961) was corrected by Muir Wood (1975) by taking into account the tangential stresses; however, the radial deformations of the tunnel lining due to these stresses were neglected. In 1976, Muir Wood (1976) solved this problem. The basis for the common tunnel design models used in practice and guidelines (ITA-WG2, 2000) were introduced by Duddeck and Erdmann (1985), including a bedded-beam model without a reduction of ground pressure at the crown and a continuum model. In the bedded-beam model, the interaction between tunnel lining and the surrounding soil is presented by bedding springs. In the continuum model, this interaction is included automatically. Blom (2002) extended a beam model to take into account the effects of longitudinal joints and soil reactions to estimate the deformation of the tunnel lining. Oreste (2007) applied a hyperstatic reaction method to derive the internal forces in the tunnel lining with a finite element method (FEM) framework for the case of tunnelling in rock. Even though the interaction between tunnel lining and surrounding medium through Winkler springs is simulated in this model, only radial pressures are considered. A further model, which includes the tangential pressures, was developed by Do et al. (2014). Recently, an adaptation of Do et al. (2014) model has been proposed by Vu et al. (2017) for shallow tunnels in soft soils. The comparison of the analytical results derived from this

* Corresponding author at: Hanoi University of Mining and Geology, Faculty of Civil Engineering, Viet Nam.
E-mail address: vuminhngan@humg.edu.vn (M.N. Vu).

https://doi.org/10.1016/j.tust.2018.04.017
Received 16 September 2017; Received in revised form 25 February 2018; Accepted 10 April 2018
Available online 16 April 2018
0886-7798/

model and Duddeck and Erdmann (1985) in Vu et al. (2017) with various depths of the tunnel shows that the new model is not only applicable in the case of shallow tunnelling and aligns closer to field observations, but also can be applied in the cases of tunnelling with moderate and deep depth.

Although many models have been proposed for tunnel design since 1926, most of these models focus on the long-term behaviours and include assumptions of the actual loading on the tunnel lining and interactions between the lining and surrounding soils that are valid for long-term loading conditions (Duddeck and Erdmann, 1985; Vu et al., 2017). In the long-term, when the grout in the tail void hardened, the tunnel lining is often considered supported directly by the soil with stresses in the soil dependent on the stress state prior to tunnelling. In practice, at the start of segment assembly, the lining is surrounded by injected grout just behind the TBM. Field data show that high pressures on the tunnel lining and large strain development occur in initial hours after assembly of tunnel segments (van Oosterhout, 2003; Bezuijen and Talmon, 2004; Talmon and Bezuijen, 2009). The other problem is that even most recent models only investigate the behaviour of the tunnel lining in a homogeneous soil and with load conditions relevant for the long-term stage. An effort to analyze the case of a tunnel in a multilayered soil was carried by Bakker (2000). However, this analysis was carried out with an approximate method by modifying the multilayered soil parameters to an approximate homogeneous soil. This might lead to inaccurate predictions of deformation and internal forces when the tunnel is in different soil layers. A numerical simulation using a 3D FE model, where the advance process of tunnelling in a two layered soil condition including the TBM advancement steps, ring-wise assembly, grout hardening process and also consolidation is modelled, will yield more detailed and more accurate results. For example, Ninić and Meschke (2017) show that such an approach is possible, but also that for engineering practice it is still less applicable due to high computational load and the required large number of input parameters. As such a simpler framework is still preferred for design purposes.

In order to prevent any damage on the tunnel lining, a careful assessment of the tunnel lining deformations and loads is needed from the time of construction to the long-term. This paper looks into a method to calculate internal forces in the long-term for a situation with multilayered soil conditions and in the tunnel lining in various construction stages as well as investigates the change of these internal forces in time.

2. Structural analysis for tunnel linings in the long-term

Recent models in tunnelling design, e.g Duddeck and Erdmann (1985), ITA-WG2 (2000), Do et al. (2014) and Vu et al. (2017), often assume a tunnel in homogeneous soil conditions. Especially, in soft soils with variable soil stiffnesses, this obviously leads to imprecise predictions for internal forces in the tunnel lining due to the inaccurate values of the interactions between the tunnel lining and the surrounding soils and the soil loading at particular points of the tunnel lining. To that end, we extend the structural model proposed in Vu et al. (2017) (Figs. 1 and 2) to the case of a multilayered soil as can be seen in Fig. 3. The lining is represented by a frame work based on the finite element (FE) model described by Do et al. (2014) and Vu et al. (2017) which is used to derive internal forces in the tunnel lining (Fig. 2).

In this model, the load at each node on the tunnel lining frame depends on the depth of the calculated ith node and which soil layer it is located. In detail, the depth of the ith node z_i is given by:

$$z_i = (H + R\cos\theta_i) \tag{1}$$

The vertical soil pressures at the ith node on the tunnel lining in the jth layer can be estimated as:

$$\sigma_{v,i} = \sum_{m=1}^{j-1} \gamma_m H_m + (z_i - H_j)\gamma_j \tag{2}$$

where H_m and γ_m are the depth and the weight unit of the mth layer (see Fig. 3).

The horizontal soil pressure at the ith node on the tunnel lining $\sigma_{h,i}$ is given by:

$$\sigma_{h,i} = K_j \sigma_{v,i} \tag{3}$$

where K_j is the coefficient of horizontal effective stress at rest of the jth layer. Adapting to the method indicated in Vu et al. (2017), the initial radial ground reaction stiffness of the jth layer $\eta_{r,j,0}$ is estimated as:

$$\eta_{r,j,0} = \beta \frac{1}{1+\nu_j}\frac{E_j}{R} \tag{4}$$

where E_j and ν_j is Young's modulus and Poisson's ratio of the jth layer and in accordance with Do et al. (2014) $\beta = 2$ is used here.

The relationship between tangential spring stiffness η_s and normal spring stiffness η_n is (Vu et al., 2017):

$$\eta_s = \frac{1}{3}\eta_n \tag{5}$$

The maximum radial reaction pressure $p_{n,j,lim}$ of the jth layer can be calculated as:

$$p_{n,j,lim} = \frac{2c_j\cos\varphi_j}{1-\sin\varphi_j} + \frac{1+\sin\varphi_j}{1-\sin\varphi_j}\Delta\sigma_{j,conf} \tag{6}$$

where c_j,φ_j are cohesion, the friction angle of the jth layer.

The confining pressure on the tunnel perimeter $\Delta\sigma_{j,conf}$ is estimated as:

$$\Delta\sigma_{j,conf} = \frac{\sigma_{h,i} + \sigma_{v,i}}{2}\frac{\nu_j}{1-\nu_j} \tag{7}$$

and the stiffness of the radial springs $k_{n,i}$ and tangential springs $k_{s,i}$ of the ith node of the frame is:

$$k_{n,i} = \eta^*_{n,j,i}\left[\frac{L_{i-1}+L_i}{2}\right] = \frac{p_{n,j,lim}}{\delta_{n,j,i}}\left(1 - \frac{p_{n,j,lim}}{p_{n,j,lim} + \eta_{n,0}\delta_{n,j,i}}\right)\frac{L_{i-1}+L_i}{2} \tag{8}$$

$$k_{s,i} = \eta^*_{s,j,i}\left[\frac{L_{i-1}+L_i}{2}\right] = \frac{p_{s,j,lim}}{\delta_{s,j,i}}\left(1 - \frac{p_{s,j,lim}}{p_{s,j,lim} + \eta_{s,0}\delta_{s,j,i}}\right)\frac{L_{i-1}+L_i}{2} \tag{9}$$

where $\delta_{n,j,i}$ and $\delta_{s,j,i}$ are the radial and tangential deformations of the ith node in the jth layer.

Similar to Do et al. (2014) and Vu et al. (2017), in this multilayered soil model, the analysis frame used consists of 360 elements representing a 1° segment. The condition that the radial springs are only active in the compression condition is still applied.

3. Structural design model for tunnel linings in construction stages

During TBM tunnelling, when precast segments are placed, the advance of the shield creates an annular cavity between the segments and the surrounding soil. This is due to the TBM's shape and the overcut. In order to minimize the movement of surrounding soil into the gap, grout is injected rapidly at the tail of the TBM. The injected grout induces pressures on the tunnel lining and the soil around. This grout pressure changes in different construction stages as shown in field data in, for example, Groene Hart Tunnel, Sophia Rail Tunnel and Botlek Railway Tunnel, in the Netherlands (van Oosterhout, 2003; Bezuijen and Talmon, 2004; Talmon and Bezuijen, 2009). Field data show that the peak value of grout pressures and the development of strains often occur in initial hours after the assembly of segments. This might lead to potential high internal forces in the tunnel lining and result in damages of the tunnel lining. A structural assessment for the tunnel lining in construction stages, therefore, can not be neglected. This part of the paper introduces a structural design model for construction stages of the tunnel lining.

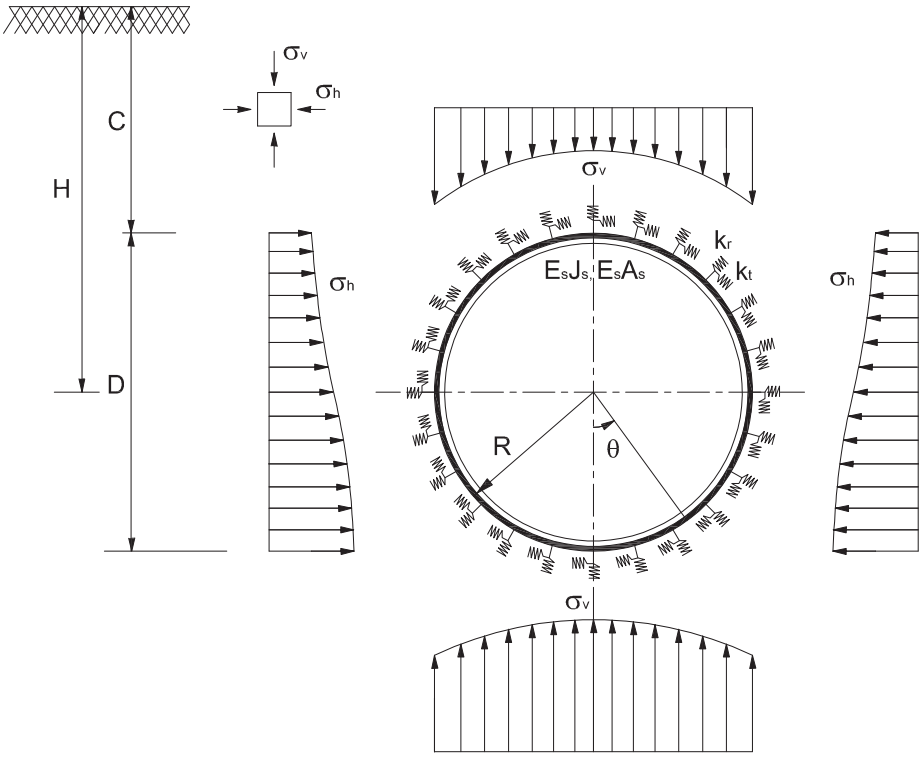

Fig. 1. Structural design model for tunnels in the long-term (Vu et al., 2017).

Based on the structural model in Section 2, analysis of construction stages is included as shown in Fig. 4. At the time of construction, it is assumed that the tunnel lining is surrounded by fluid grout instead of the soil. The tunnel lining at this moment is directly loaded by grout pressures.

The applicable range of grouting pressures on the tunnel lining that might occur in the time of construction is estimated here from the stability analysis in Vu et al. (2015). Since the grouting pressures reduce along the tunnel lining in time as the grout hardens, the grouting pressures are derived from the initial grout pressure by taking an appropriate percentage of the initial support pressures at the tail in analysis for each construction stage, as can be seen in Fig. 5. Field data from Groene Hart Tunnel, Sophia Rail Tunnel and Botlek Railway Tunnel in van Oosterhout (2003), Bezuijen and Talmon (2004) and Talmon and Bezuijen (2009) shows that after peak values in the initial hours after assembly of the segments, the pressure on the tunnel lining trends towards the initial soil stresses, which are used in long-term calculation as indicated in recent models as Duddeck and Erdmann (1985), ITA-WG2 (2000), Do et al. (2014) and Vu et al. (2017). Therefore, it can be assumed that in the hardening phase of the grout, the tunnel lining is loaded by grout pressure and after grout hardening, the hardened grout can be considered as a part of lining segments and the tunnel lining is loaded by initial soil stress in the long-term.

In the construction stage model, the spring stiffness is estimated by interactions between the grout and the tunnel lining. The method of calculating the interaction between the tunnel lining and surrounding medium in Vu et al. (2017) is adapted for the case of the tunnel lining surrounded by the grout. The grout stiffness is derived from calculations in Kasper and Meschke (2004) and experimental data as indicated in Hashimoto et al. (2005), such that the apparent stiffness of the grout η^*_{gr} is calculated as:

$$\eta^*_{gr} = \frac{p_{gr,lim}}{\delta}\left(1-\frac{p_{gr,lim}}{p_{gr,lim}+\eta_{gr,0}\delta}\right) \tag{10}$$

where $p_{gr,lim}$ is the maximum reaction pressure that the grout can offer

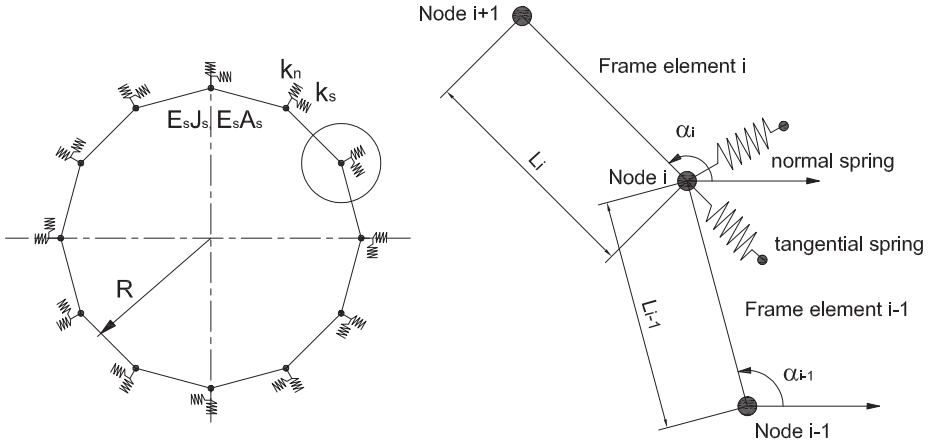

Fig. 2. FE model for structural analysis for tunnels in Vu et al. (2017).

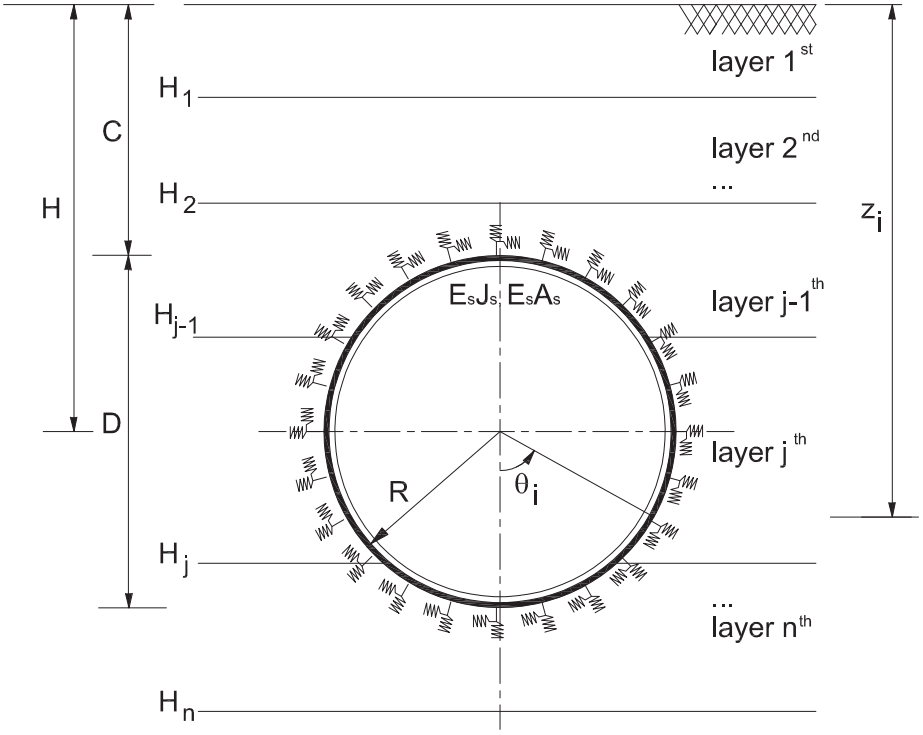

Fig. 3. A tunnel lining in multilayered soil condition.

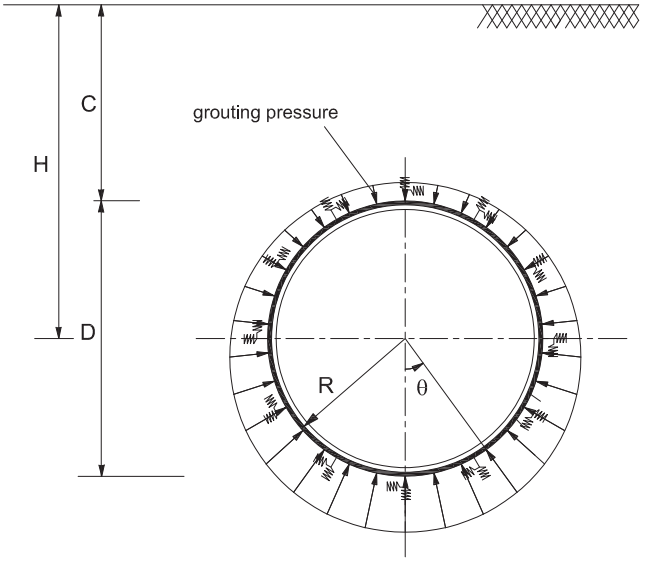

Fig. 4. Grouting pressures around the tunnel lining.

and $\eta_{gr,0}$ is the stiffness of the grout, derived from the modulus of elasticity of the grout during the construction stage.

The radial grout reaction stiffness $\eta_{r,gr,0}$ is estimated as:

$$\eta_{r,gr,0} = \beta \frac{1}{1+\nu_{gr}} \frac{E_{gr}}{R} \tag{11}$$

where E_{gr} is the elastic modulus of the grout at the construction stage and ν_{gr} is Poisson's ratio of the grout.

The relationship between tangential spring stiffness η_s and normal spring stiffness η_n is:

$$\eta_s = \frac{1}{3}\eta_n \tag{12}$$

The maximum radial reaction pressure $p_{n,gr,lim}$ in Eq. (10) can be given by:

$$p_{n,gr,lim} = \frac{2c_{gr}\cos\varphi_{gr}}{1-\sin\varphi_{gr}} + \frac{1+\sin\varphi_{gr}}{1-\sin\varphi_{gr}}\Delta\sigma_{gr,conf} \tag{13}$$

where c_{gr} is cohesion of the grout, φ_{gr} is the friction angle of the grout and $\Delta\sigma_{gr,conf}$ is the confining pressure on the tunnel perimeter estimated as:

$$\Delta\sigma_{gr,conf} = \frac{\sigma_h + \sigma_v}{2}\frac{\nu_{gr}}{1-\nu_{gr}} \tag{14}$$

The maximum shear reaction pressure on the tunnel lining $p_{s,gr,lim}$ is given by:

$$p_{s,gr,lim} = \frac{\sigma_h + \sigma_v}{2}\tan\varphi_{gr} \tag{15}$$

The stiffness of the radial springs $k_{n,i}$ and tangential springs $k_{s,i}$ in each elements of the frame is:

$$k_{n,i} = \eta^*_{n,gr,i}\left[\frac{L_{i-1}+L_i}{2}\right] = \frac{p_{n,gr,lim}}{\delta_{n,i}}\left(1-\frac{p_{n,gr,lim}}{p_{n,gr,lim}+\eta_{n,0}\delta_{n,i}}\right)\frac{L_{i-1}+L_i}{2} \tag{16}$$

$$k_{s,i} = \eta^*_{s,gr,i}\left[\frac{L_{i-1}+L_i}{2}\right] = \frac{p_{s,gr,lim}}{\delta_{s,i}}\left(1-\frac{p_{s,gr,lim}}{p_{s,gr,lim}+\eta_{s,0}\delta_{s,i}}\right)\frac{L_{i-1}+L_i}{2} \tag{17}$$

where L_i is the distance between the ith node and the $(i+1)$th node (see Fig. 2).

4. Validations with case studies

4.1. A tunnel in multilayered soil

In order to validate the proposed multilayered soil model, a case study of the Second Heinenoord Tunnel, the Netherlands, which was extensively documented in Bakker (2000, 2003) and Vu et al. (2017) is used. This tunnel with an outer diameter of 8.3 m was constructed below the Oude Maas river in Rotterdam in the period from 1996 to

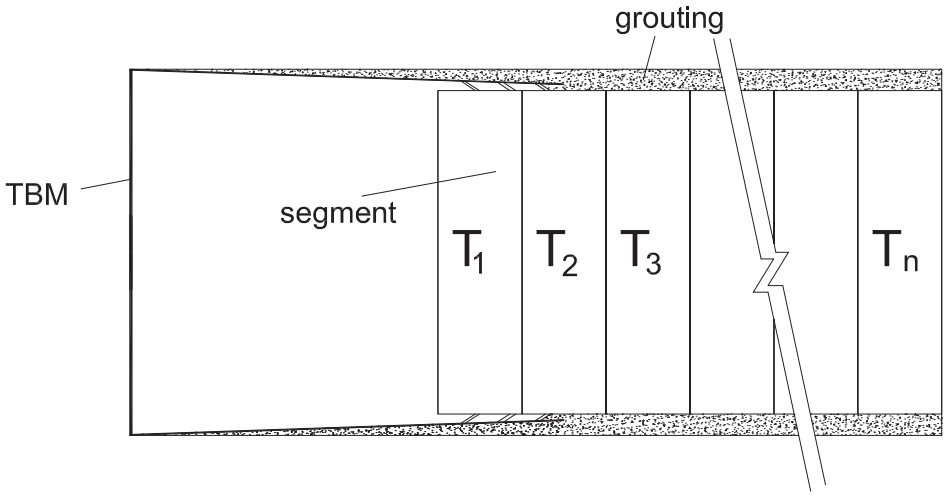

Fig. 5. Time steps of tunnel segment assembly.

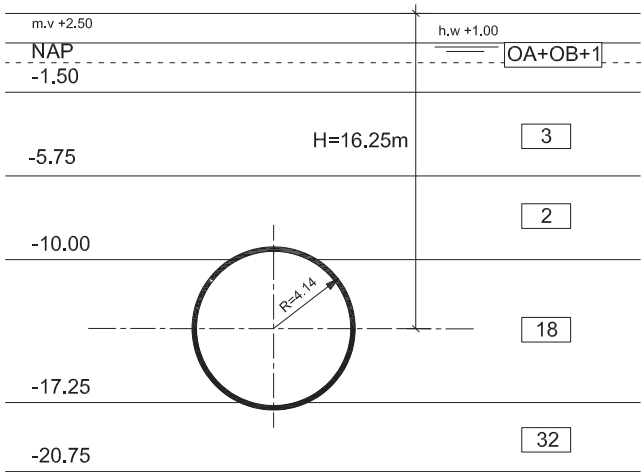

Fig. 6. Cross-section of the measured location in the North Bank in Second Heinenoord Tunnel (figure adapted by authors from Bakker (2003)).

1999. The monitoring was carried out in this project at two measurement locations on the North Bank and on the South Bank. Measurement instruments were installed in all seven elements of a ring in order to derive the stress distribution in the ring. Internal forces in the tunnel lining were measured by using strain gauges during the construction. Field observations were performed with a cross-section of the tunnel on the North Bank where the tunnel axis is located at about 16.25 m below the surface with a tunnel diameter of 8.3 m (see Fig. 6) at the time steps of 9 days and 330 days after assembly of the lining segments. Calculations are carried out with the proposed multilayered soil model with the input parameters as shown in Fig. 6 and Table 1. Results derived from the proposed multilayered soil model are compared with the results from models proposed in Duddeck and Erdmann (1985) and Vu et al. (2017), a 3D FEM analysis using ANSYS in Bakker (2000), a 2D Plaxis FEM model in Bakker (2003) and the field data after 330 days as shown in Figs. 7 and 8.

Fig. 7 presents a comparison of bending moments from the field data and the bending moments derived from Duddeck and Erdmann (1985), Vu et al. (2017), Bakker (2003) 2D Plaxis model, Bakker (2000) ANSYS model and the new multilayered soil model. It can be seen that the bending moments estimated from these models share a trend with the observed data. The bending moments derived from the new multilayered soil model, Duddeck and Erdmann (1985), Vu et al. (2017) and Bakker (2000) ANSYS model all correspond well with the peak in a highest bending moment observed in the field data at the location of 166° on the tunnel's cross-section. The bending moments derived by Bakker (2003) are more in line with the low bending moment observed is most other points of the cross-section.

In the comparison of normal forces as shown in Fig. 8, the normal forces derived from the new multilayered soil model show a similar variation as the analytical results estimated from Duddeck and Erdmann (1985), Vu et al. (2017) and Bakker (2003) 2D Plaxis model but a larger offset. Interestingly, most of the observed peaks of normal force in the field data are close to the normal forces derived from the new multilayered soil model while there exists a marked difference between the field data and results derived from Bakker (2003) which significantly underestimates the normal forces. Normal forces derived from the proposed model are close to the field data observations with peak normal forces from observed field data underestimated less than 10%, whereas,for other models, these are more than 25%

Table 1
Description of layers and soil parameters for the North Bank of the Second Heinenoord Tunnel (Data from Bakker (2000)).

Symbol	Soil type	Top of layer (m) N.A.P	Unit weight γ_{wet} (γ_{dry}) (kN/m^3)	Undrained shear strength c_u (kPa)	Cohesion c' (kPa)	Friction angle φ^{prime} (deg.)	Possion's ratio ν (–)	Elastic modulus E (MPa)	Earth pressure coefficient K_0 (–)
$OA + OB + 1$	Mixture of sand and clay	+2.50	17.2(16.5)	–	3	27	0.34	5.2	0.58
3	Sand, local parts of clay	−1.50	19.5	–	0	35	0.3	26	0.47
2	Sand with clay	−5.75	19	–	0	33	0.31	25	0.47
18	Sand, local parts of clay	−10.00	20.5	–	0	36.5	0.3	40	0.45
32	Sand, gravel	−17.25	20.5	–	0	36.5	0.3	60	0.5

Note: OA,OB = man-made fills; N.A.P. = Nieuw Amsterdam Peil (Dutch reference level, approx. mean sea level).

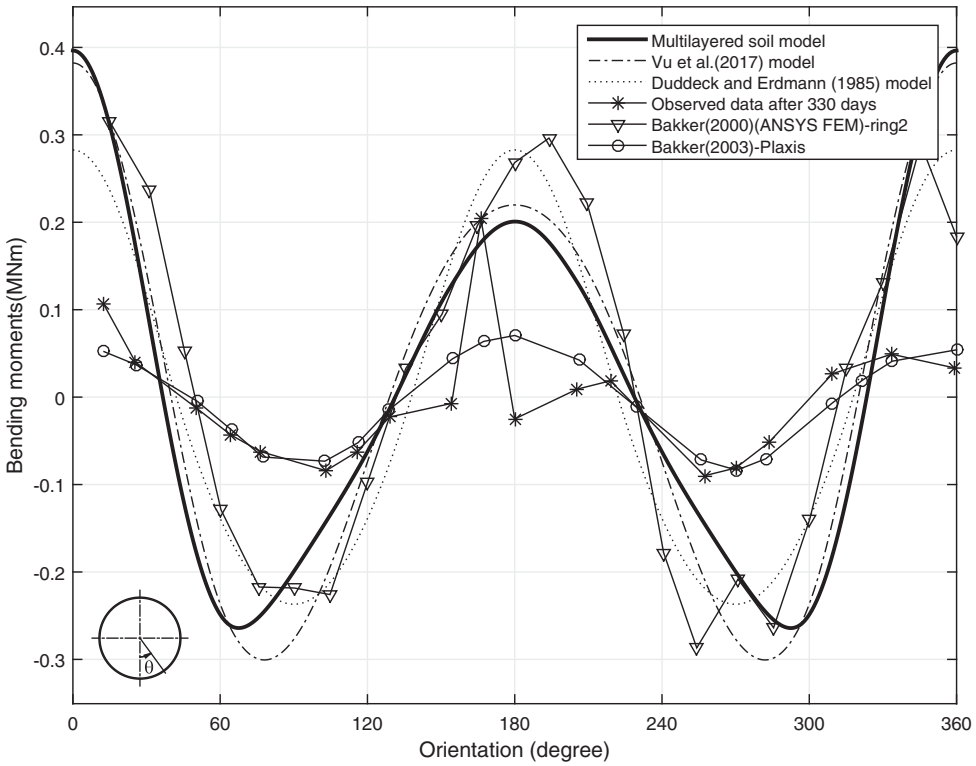

Fig. 7. Validation of bending moments in Second Heinenoord Tunnel after 330 days.

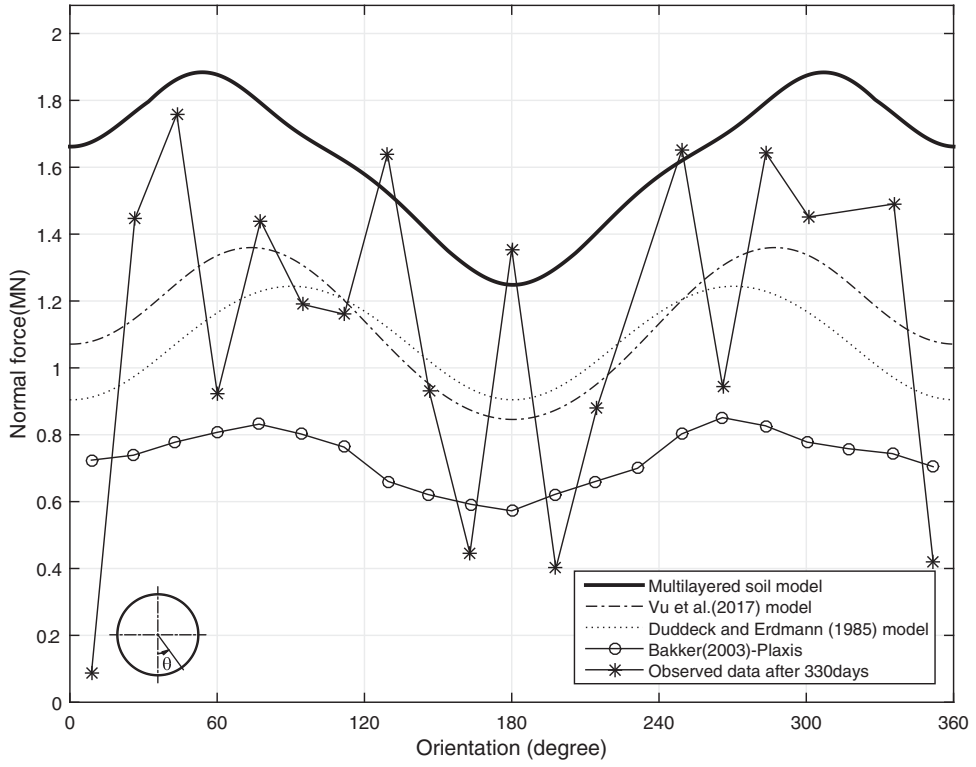

Fig. 8. Validation of normal forces in Second Heinenoord Tunnel after 330 days.

underestimated. The new multilayered soil model can predict potential normal forces in the lining more conservatively than the other models.

Table 2 lists the overall agreement between model results and observed data as overall coefficients of determination R_M^2 and R_N^2 for bending moments and normal forces to give an indication of the global fit between model and observed data. It also shows the ratio $M_{model,max}/M_{obs,max}$ between the maximum modelled over maximum observed bending moments near the crown of the tunnel (around 180°) and $N_{model,max}/N_{obs,max}$ for the normal forces for the peak values.

R_M^2 and R_N^2 are given by:

Table 2
Agreements between model results and observed lining behaviour at Second Heinenoord Tunnel for the various models.

Model	R_M^2 for M	$M_{model,max}/M_{obs,max}$	R_N^2 for N	$N_{model,max}/N_{obs,max}$
After 9 days				
Multilayered	0.667	1.105	−9.34	0.715
After 330 days				
Multilayered	0.337	0.985	−10.52	1.068
Vu et al. (2017)	0.346	1.079	−5.33	0.773
Duddeck and Erdmann (1985)	0.416	1.388	−10.19	0.707
Bakker (2003) Plaxis	0.260	0.313	−49.78	0.484
Bakker (2000) ANSYS FEM	0.398	1.318	–	–

$$R_M^2 = 1 - \frac{\sum (M_{model,i} - M_{obs,i})^2}{\sum (M_{model,i} - \overline{M_{model}})^2} \tag{18}$$

$$R_N^2 = 1 - \frac{\sum (N_{model,i} - N_{obs,i})^2}{\sum (N_{model,i} - \overline{N_{model}})^2} \tag{19}$$

where

$$\overline{M_{model}} = \frac{1}{n} \sum_{i=1}^{n} M_{model,i} \tag{20}$$

$$\overline{N_{model}} = \frac{1}{n} \sum_{i=1}^{n} N_{model,i} \tag{21}$$

Except for the Plaxis model in Bakker (2003), all models overestimate the average bending moments M, and underestimate the maximum normal forces N. The multilayer model is somewhat more conservative in these respects than similar models for a first estimate of maximum M and N. For a more detailed analysis, a 3D or multi-ring FE model would be needed. However, the poor overall correspondence between models and field observations, as highlighted by the low R_M^2 values for bending moments and the extremely poor, negative, values for normal forces, indicates most probably that installation effects play a major role in the acting lining forces.

Based on these validations, it can be concluded that the predicted internal forces derived from the new multilayered soil model are generally in accordance with the field data and are more conservative than the other models.

4.2. For multiple construction stages

The validation of the model for construction stages is performed with two case studies of Second Heinenoord Tunnel and Botlek Railway Tunnel, in the Netherlands (Bakker, 2000, 2003; Blom, 2002).

4.2.1. Second Heinenoord Tunnel

The validation for the construction stage model is carried out with the case of Second Heinenoord Tunnel as indicated above (see in Fig. 6) at 9 days after assembly of the tunnel segments with the description of soil layers and soil parameters of the case study of Second Heinenoord Tunnel shown in Table 1. At this time, the grout stiffness $E_{gr} = 3MPa$ and the grout pressures at the top and the bottom of the tunnel in the model is equal to the initial soil pressures at these points. The internal forces derived from the construction stage model are compared to field data in Bakker (2003).

Figs. 9 and 10 show a comparison between bending moments and normal forces derived from the construction stage model and observed data. It can be seen that the bending moments derived from the construction stage model are in line with the observed data in Fig. 9. The peak bending moment at 166° is nearly equal to the bending moment estimated by the model. The bending moments of this peak increase from 0.15 to 0.2 MN m between 9 and 330 days as can be observed from Fig. 7. The construction stage model can well predict the bending moments in this case.

The plot of normal forces in Fig. 10 also shows a good agreement between the normal forces calculated from the construction stage model and field data. Most of the field data is close to the analysis results, although the correspondence is not as respective as for the bending moments.

4.2.2. Botlek Railway Tunnel

Further validation for the construction stage model is performed with a case study of the Botlek Railway Tunnel in the Netherlands. This

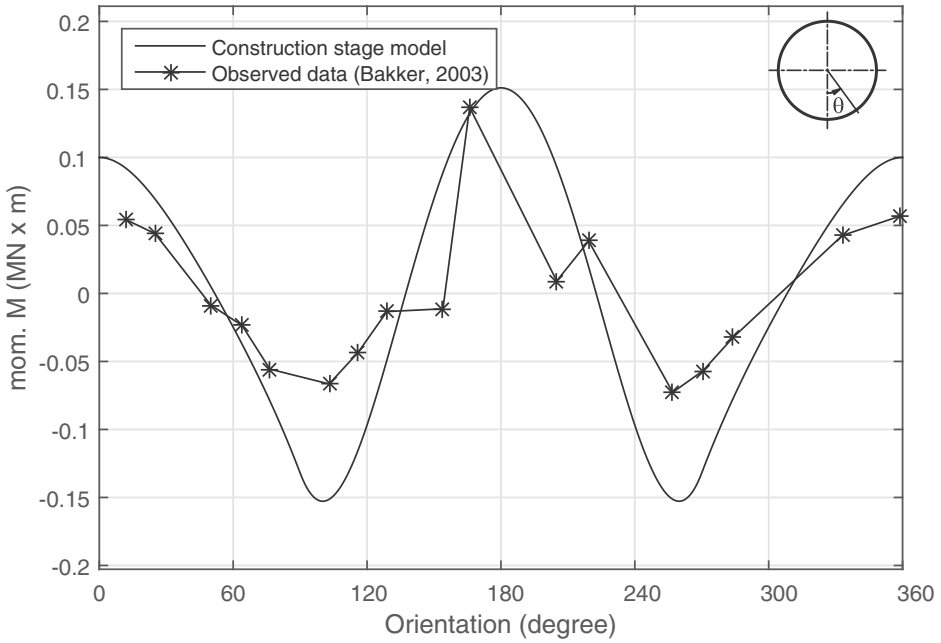

Fig. 9. Validation of bending moments in Second Heinenoord Tunnel after 9 days.

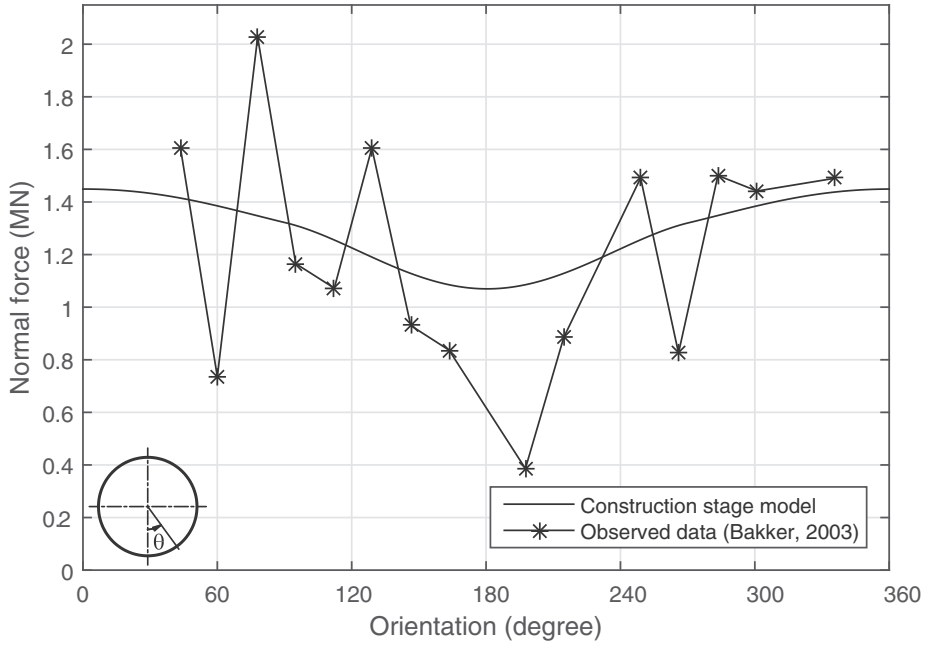

Fig. 10. Validation of normal forces in Second Heinenoord Tunnel after 9 days.

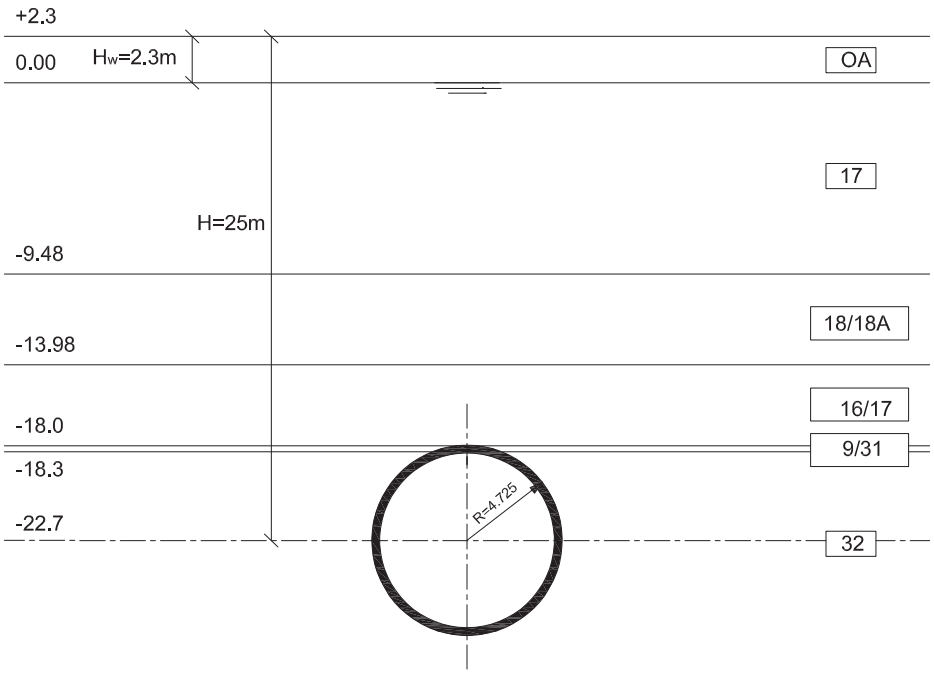

Fig. 11. Geometry of Botlek Railway Tunnel.

is a shield driven tunnel below the river Oude Maas in Rotterdam, with two tubes of 1800 m length. The external diameter of the tunnel lining is 9.45 m with a thickness of 0.40 m. A ring in the Botlek Railway Tunnel consists of 7 segments and a keystone. Structural health monitoring instruments were installed in the northern tube in order to monitor structural behaviour of the tunnel lining. The monitoring work concentrated on the initial steps of the tunnel lining from the assembly of the ring in the TBM to the following days when the tunnel lining is loaded by liquid grout. The monitoring consisted of strain measurements both in tangential and axial directions. The monitoring results show that the assembly and the subsequent first day are the most significant in the strain development in a tunnel lining.

The geometry of Botlek Railway Tunnel in this analysis are shown in Fig. 11 and Table 3. The tunnel is located $H = 25$ m below the surface with the water level at $H_w = 2.3$ m below the surface and input soil parameters as shown in Table 3.

The analysis is carried out at three moments after the assembly of the segments in the TBM and compared with observed data in Blom (2002) at $T = 350$ (5 h 50 min), $T = 750$ (12 h 30 min) and $T = 7500$ min (5 days 5 h).

At $T = 350$ min, grout pressures are modelled equal to the maximum support pressures at the top and the bottom of the tunnel lining as derived from Vu et al. (2015), as the tunnel lining is at the tail of the TBM. From the observed field data, grout pressures at the time step $T = 750$ min can be calculated as about 85% of the maximum support pressures at the top and the bottom of the tunnel lining used in the time

Table 3
Description of layers and soil parameters for the Botlek Railway Tunnel (Data from Feddema (2002)).

Symbol	Soil type	Top of layer (m) N.A.P	Unit weight γ_{wet} (γ_{dry}) (kN/m^3)	Undrained shear strength c_u (kPa)	Cohesion c' (kPa)	Friction angle φ' (deg.)	Possion's ratio ν (–)	Elastic modulus E (MPa)	Earth pressure coefficient K_0 (–)
OA	Sand/clay	+2.30	17(15.3)	–	3.5	25	0.2	8	0.62
17	Clay with sand	−9.48	19	–	5	27.5	0.2	8	0.54
18/18*A*	Holoceen sand/ clayey sand	−13.98	19	–	0	34.5	0.2	19	0.58
16/17	Clay, sandy clay	−18	17	–	7.5	23.8	0.2	7.7	0.58
9/31	Clay, silt local parts of clay	−18.3	11	–	10	25	0.2	3.75	0.36
32	Pleistoceen sand, gravel	−27.4	20	–	0	34	0.2	54	0.46

Note: OA = man-made fills; N.A.P. = Nieuw Amsterdam Peil (Dutch reference level, approx. mean sea level).

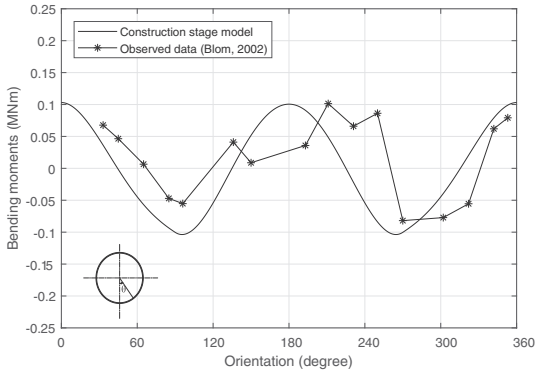

(a) T=350 min

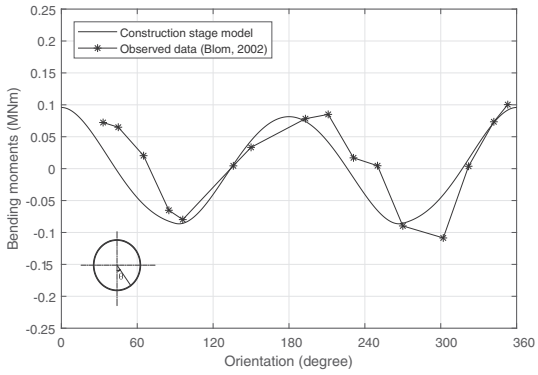

(b) T=750 min

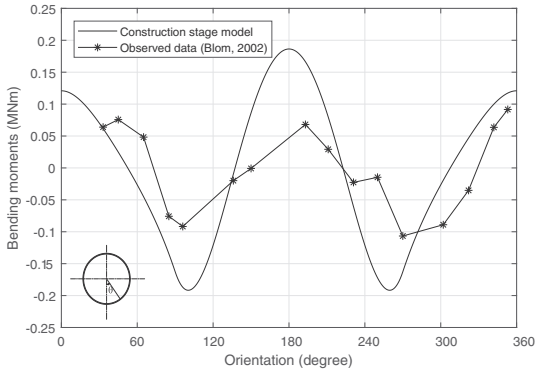

(c) T=7500 min

Fig. 12. Validation of bending moments in Botlek Railway Tunnel.

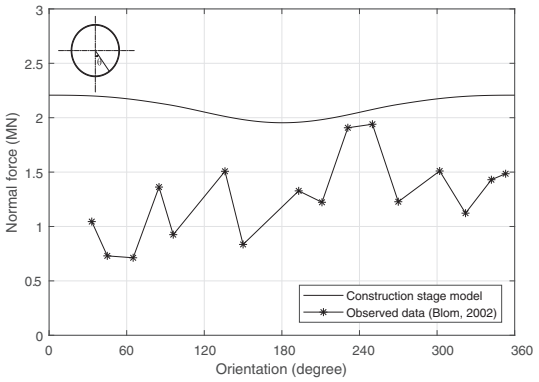

(a) T=350 min

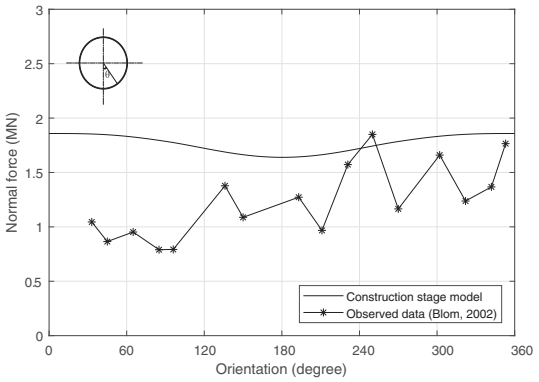

(b) T=750 min

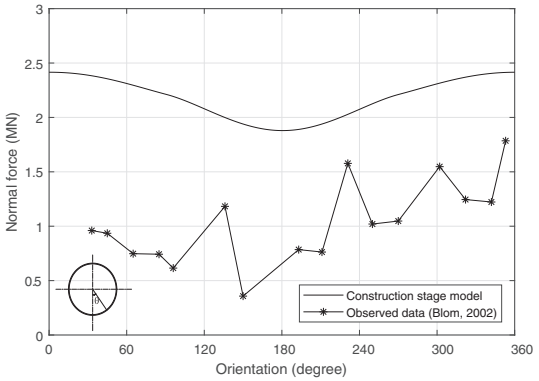

(c) T=7500 min

Fig. 13. Validation of normal forces in Botlek Railway Tunnel.

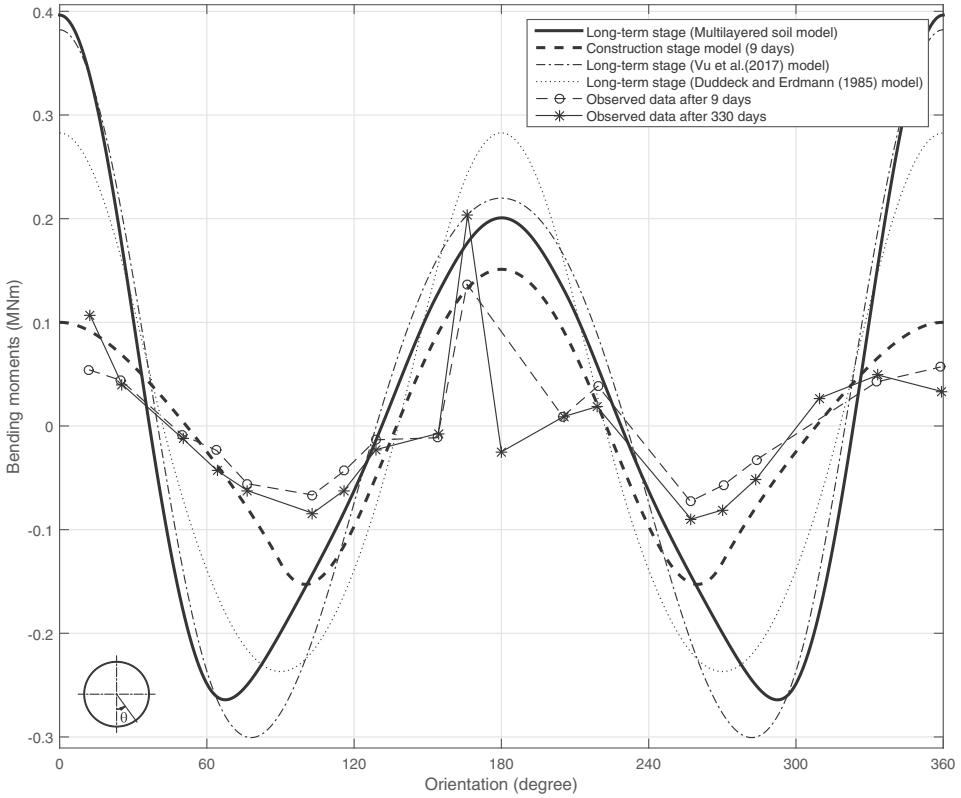

Fig. 14. Changes of bending moments in the tunnel lining in Second Heinenoord Tunnel.

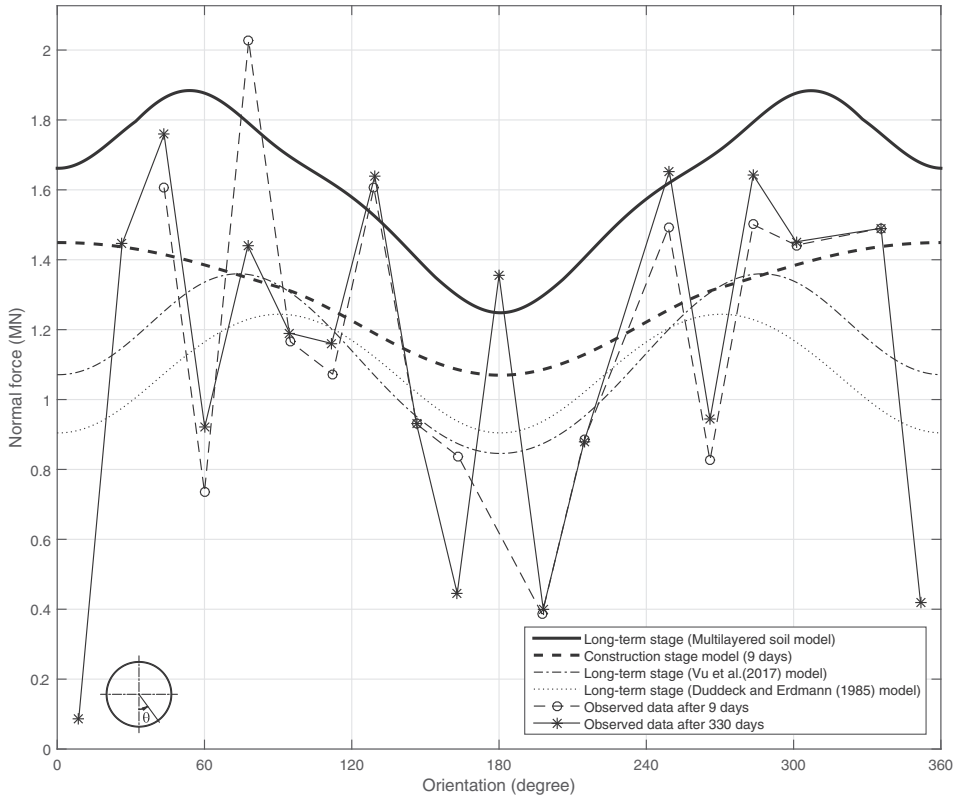

Fig. 15. Changes of normal forces in the tunnel lining in Second Heinenoord Tunnel.

step $T = 350$ min. The observed data in Botlek Tunnel, Groene Hart Tunnel and Sophia Rail Tunnel (Bezuijen and Talmon, 2004; Talmon and Bezuijen, 2009) show that the grout pressure becomes close to the initial soil pressure after two days from the assembly. Grout pressures at the top and bottom of the tunnel lining used to analyse at $T = 7500$ min in the model, therefore, are equal to the initial soil pressures at these points.

The grout stiffness is estimated as indicated by Meschke et al. (1996) and from the data in Hashimoto et al. (2005). The stiffness of the grout E_{gr} at the time steps $T = 350$ min,750 min and 7500 min is taken equal to 0.125 MPa, 0.2 MPa, and 2.0 MPa, respectively.

A comparison of the bending moments is shown in Fig. 12. This figure shows that bending moments derived from the proposed model have the same trend and are close to the field data at the time steps $T = 350$ min and $T = 750$ min for most points in the tunnel cross-section. For the peak observed value near $\theta = 210°$ $M_{model,max}/M_{obs,max}$ ratios of 1.0 and 0.96 are derived. At the time step $T = 7500$ min, the observed bending moments at the bottom of the tunnel lining are still close to the predicted bending moments derived from the model although there is an overestimation of the bending moments at the sides and crown of the tunnel, up to a $M_{model,max}/M_{obs,max}$ ratio of 2.75.

Fig. 13 shows a comparison of normal forces. Overall, normal forces from the proposed model exceed the field data observations with peak normal forces from observed field data overestimated less than 20% but average normal force overestimated roughly 50%. For $T = 350$,750 and 7500 min $N_{model,max}/N_{obs,max}$ ratios of 1.14, 0.95 and 1.35 respectively are derived. When comparing to the Second Heinenoord Tunnel case, we see an overestimate of the predicted normal forces, but again the proposed model reliably predicts the value of the bending moments in different construction stages.

These results show that the proposed model can satisfactorily predict bending moments and to a lesser extent normal forces of the lining in different construction stages.

5. Changes of internal forces from the time of construction to the long-term

In order to understand the change of the internal forces in the tunnel lining from the time of construction to the long-term, analytical results derived from Duddeck and Erdmann (1985) and Vu et al. (2017), the construction stage model and the multilayered soil model are combined with field data in the case study of Second Heinenoord Tunnel at time steps of 9 days and 330 days.

Fig. 14 shows the change of bending moments in the tunnel lining. It can be seen that from 9 to 330 days after assembly, the observed bending moment in the tunnel lining shows a slight increase. This increase is also found in the new model, although it is far more pronounced there. The new model would correspond well with peak measured bending moments in this case. Just after segment assembly, the lining is surrounded by the injected grout and is under grout pressure. After the hardening of the grout, it can be considered that the grout becomes a part of the lining and the lining-grout system is loaded by the initial soil pressures.

Fig. 15 shows the change of normal forces in the tunnel lining at these times. It can be seen from this figure that the normal forces derived from the construction stage model are close to the normal forces derived from Duddeck and Erdmann (1985) and Vu et al. (2017) and also have a good agreement with the values in field data. Meanwhile, the normal forces derived from the multilayered long-term model are close to the high observed normal force in field data. The increase of normal forces calculated between the construction stage and the long-term is also seen in the field data at the cross-section. This means that proposed models in this paper can predict internal forces in the tunnel lining from the construction stages to the permanent stage and are more accurate for short-term loading than earlier models as well as are still conservative with respect to long-term loading conditions.

6. Conclusion

The tunnel lining should be designed for both the short-term construction stages and the long-term because field data show high pressures and strain development in the initial hours after segment assembly. Taking into account the interaction between the tunnel lining and surrounding grout and multiple soil layers, this paper derives internal forces in the tunnel lining not only for construction stages but also for the long-term. The analysis shows a good agreement between the results derived from the new models and field data and shows that the impact of accurately including short-term load conditions such as liquid grout in the tail void has a more significant impact on internal forces in the lining than including multilayered soils. It is also shown that internal forces in the tunnel lining increase in time after the initial grout loading and become stable in the long-term. The new combined model provides a conservative estimate for the long-term load that is comparable with similar models and in current tunnel design practice.

Appendix A. Supplementary material

Supplementary data associated with this article can be found, in the online version, at http://dx.doi.org/10.1016/j.tust.2018.04.017.

References

Bakker, K.J., 2000. Soil Retaining Structures: Development of Models for Structural Analysis. Ph.D. thesis, Delft University of Technology.

Bakker, K.J., 2003. Structural design of linings for bored tunnels in soft ground. Heron 48 (1), 33–64.

Bezuijen, A., Talmon, A., 2004. Grout pressures around a tunnel lining, influence of grout consolidation and loading on lining. Tunn. Decade Prog. GeoDelft 109–114.

Blom, C.B.M., 2002. Design Philosophy of Concrete Linings for Tunnels in Soft Soils. Ph.D. thesis, Delft University of Technology.

Broere, W., 2016. Urban underground space: solving the problems of today's cities. Tunn. Undergr. Space Technol. 55, 245–248.

Do, N.A., Dias, D., Oreste, P., Djeran-Maigre, I., 2014. A new numerical approach to the hyperstatic reaction method for segmental tunnel linings. Int. J. Numer. Anal. Methods Geomech. 38 (15), 1617–1632.

Duddeck, H., Erdmann, J., 1985. Structural design models for tunnels in soft soil. Undergr. Space (United States) 9.

Feddema, A., 2002. Postdicties met het groutdrukmodel aan de hand van metingen bij de botlekspoortunnel (f330). Tech. Rep., GeoDelft.

Hashimoto, T., Konda, T., Brinkman, J., Feddema, A., Kano, Y., 2005. Simultaneous backfill grouting, pressure development in construction phase and in the long-term. Tunn. Decade Prog. GeoDelft 1995–2005, 101.

ITA-WG2, 2000. Guidelines for the design of shield tunnel lining. Tunn. Undergr. Space Technol. 15(3), 303–331.

Kasper, T., Meschke, G., 2004. A 3D finite element simulation model for TBM tunnelling in soft ground. Int. J. Numer. Anal. Methods Geomech. 28 (14), 1441–1460.

Meschke, G., Kropik, C., Mang, H., 1996. Numerical analyses of tunnel linings by means of a viscoplastic material model for shotcrete. Int. J. Numer. Methods Eng. 39 (18), 3145–3162.

Morgan, H., 1961. A contribution to the analysis of stress in a circular tunnel. Geotechnique 11 (1), 37–46.

Muir Wood, A., 1975. The circular tunnel in elastic ground. Geotechnique 25 (1), 115–127.

Muir Wood, A., 1976. Discussion: the circular tunnel in elastic ground. Geotechnique 26 (1), 231–237.

Ninić, J., Meschke, G., 2017. Simulation based evaluation of time-variant loadings acting on tunnel linings during mechanized tunnel construction. Eng. Struct. 135, 21–40.

Oreste, P., 2007. A numerical approach to the hyperstatic reaction method for the dimensioning of tunnel supports. Tunn. Undergr. Space Technol. 22 (2), 185–205.

Schmid, H., 1926. Statische Probleme des Tunnel-und Druckstollenbaues und ihre gegenseitigen Beziehungen. Springer.

Schulze, H., Duddeck, H., 1964. Spannungen in schildvorgetriebenen tunneln. Beton-und Stahlbetonbau 59 (8), 169–175.

Talmon, A., Bezuijen, A., 2009. Simulating the consolidation of TBM grout at noordplaspolder. Tunn. Undergr. Space Technol. 24 (5), 493–499.

van Oosterhout, G., 2003. Recent dutch experiences in developing structural monitoring systems tor shield driven tunnels. HERON 48 (1).

Vu, M.N., 2016. Reducing the Cover-to-diameter Ratio for Shallow Tunnels in Soft Soils. Ph.D. thesis, Delft University of Technology.

Vu, M.N., Broere, W., Bosch, J.W., 2015. The impact of shallow cover on stability when tunnelling in soft soils. Tunn. Undergr. Space Technol. 50, 507–515.

Vu, M.N., Broere, W., Bosch, J.W., 2017. Structural analysis for shallow tunnels in soft soils. Int. J. Geomech. 17 (8).

Windels, R., 1966. Spannungstheorie zweiter ordnung für den teilweise gebetteten kreisring. Die Bautechnik 43, 265–274.

Windels, R., 1967. Kreisring im elastischen kontinuum. Der Bauingenieur Bd 42, 429.